Available online at www.sciencedirect.com
ScienceDirect
Trans. Nonferrous Met. Soc. China 32(2022) 319−332
Transactions of Nonferrous Metals Society of China
www.tnmsc.cn

# Hydrometallurgical process for extracting bismuth from by-product of lead smelting based on methanesulfonic acid system

Tian-xiang NAN[1], Jian-guang YANG[1], Chao-bo TANG[1], Wen-chao WANG[1], Wei LONG[1], Ji-yuan YANG[2]

1. School of Metallurgy and Environment, Central South University, Changsha 410083, China;
2. Queen Mary University of London Engineering School, Northwestern Polytechnical University, Xi'an 710129, China

Received 27 November 2020; accepted 29 June 2021

**Abstract:** A new hydrometallurgical process based on the methanesulfonic acid system was proposed to extract the bismuth efficiently from by-products of lead smelting. The bismuth extraction process included electrorefining, oxidation leaching, and electrodeposition. The optimum conditions of the bismuth extraction process were determined by a single-factor test. The bismuth plate with a purity of 99.8% was obtained under the optimum conditions. Cyclic voltammetry and linear sweep voltammetry were applied to investigating the cathode reaction mechanism of electrorefining. The results show that lead deposition, bismuth deposition, and hydrogen evolution occur at the cathode, and the reactions of metals deposition are irreversible and diffusion-controlled. In addition, decreasing the temperature and acidity can improve the purity of the cathodic product (lead powder) in the electrorefining process.
**Key words:** bismuth; hydrometallurgical process; methanesulfonic acid system; electrochemical mechanism

## 1 Introduction

Lead concentrate and secondary lead-bearing resources, containing lead and other valuable metals such as antimony, bismuth, arsenic, copper, and silver, are the primary raw materials for lead smelting [1,2]. Most valuable metals fall off during the electrorefining process along with a small amount of undissolved lead, forming the anode slime, which is usually smelted to separate and recover the valuable metals with high added value [3]. A certain amount of lead alloy is produced at the bottom of the furnace and accumulates as the smelting continues. Some problems can arise with the increase of alloy's volume, such as low smelting efficiency and equipment corrosion. Therefore, it is necessary to recycle the alloy at the bottom of the furnace after a particular production period [4]. The recovery of bismuth from the alloy is significant because there is a large amount of bismuth in the alloy, usually more than 20% [5].

Nowadays, the main methods for the extraction and recovery of bismuth include hydrometallurgy [6], pyrometallurgy [7], and physical method [8]. HE et al [9] proposed the technology of lead anode slime treatment by "pressure oxidation alkaline leaching—crude bismuth alloy casting—bismuth electrolysis" process, with the recovery rate of bismuth over 98%. CHEN et al [10] studied a bismuth recovery technology in the $H_2SO_4$−NaCl system, and the sponge bismuth with a purity of 90% was obtained after leaching and filtration. LUCHEVA et al [11] reported carbon thermal reduction for the recovery of copper ash-bearing bismuth and lead. After the pretreatment process (leaching by NaOH) and reduction smelting process, the yield rates of bismuth and lead reached 65% and 80%, respectively.

**Corresponding author:** Jian-guang YANG, Tel: +86-731-88830470, E-mail: jianguang_y@163.com
DOI: 10.1016/S1003-6326(22)65797-2

It is difficult to recover bismuth from the lead-based alloy. Although antimony can be recovered effectively by pyrometallurgy, it is challenging to separate lead and bismuth [12,13]. The hydrometallurgical separation method has the disadvantages of low leaching rate and long reaction time. Also, high content of bismuth in the alloy limits the traditional electrorefining in a silicofluoric acid system [14−16]. In this work, an "electrorefining — oxidation leaching — electrodeposition" process was proposed based on methanesulfonic acid (MSA) system, which can extract high-purity bismuth efficiently when obtaining crude lead powder and antimony residue. First of all, The MSA solution can dissolve lead and bismuth selectively to separate antimony [17]. Secondly, the lead electrorefining in the MSA system can effectively avoid anode passivation caused by high bismuth content. Finally, it is an environmentally friendly process that can reduce waste water through solution recycling.

## 2 Experimental

### 2.1 Materials, reagents, and equipment

Raw materials used in this study are the lead alloy from the bottom of the furnace, resulting from the smelting process of the anode slime in a lead-smelting enterprise in China. The variety and content of metallic elements in the homogenized sample of lead-based alloy scraps are shown in Table 1.

**Table 1** Main element content of lead alloy bearing high antimony and bismuth (wt.%)

| Sb | Bi | Pb | Cu | Ag |
|---|---|---|---|---|
| 15.70 | 22.20 | 61.20 | 0.71 | 0.14 |

All reagents, including $CH_4O_3S$, $H_2O_2$, $Bi_2O_3$, and PbO are analytically pure. The solutions for electrolysis and leaching were prepared using distilled water. The temperature control equipment was the DF−101S magnetic water bath kettle. IT6721 DC power was used for electrolysis, and the electrochemical test was conducted on the Chenhua CHI670E electrochemical workstation.

### 2.2 Process experiment

2.2.1 Procedure

Figure 1 illustrates the experiment flow chart. The lead methanesulfonate solution was used as the electrolyte for electrorefining, and the products of anode and cathode were bismuth-rich anode slime and raw lead powder, respectively. With hydrogen peroxide as the oxidant, the bismuth-rich anode slime was leached by MSA solution. The antimony and silver were recovered firstly from the leaching residue. After that, the electrodeposition process was carried out on the leaching solution, and then the electrolyte was recovered and used to leach bismuth-rich anode slime. Therefore, in theory, this process took place in a closed circuit.

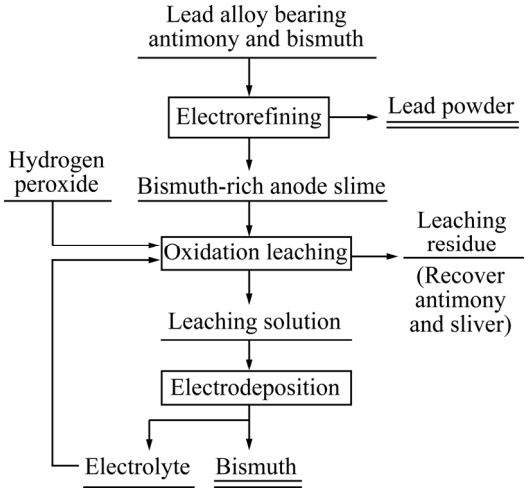


**Fig. 1** Experiment flow chart

2.2.2 Electrorefining

Lead-based alloy and graphite plate were served as anode and cathode, separately. The electrolyte was prepared with MSA and PbO, and the initial concentration of $Pb^{2+}$ was 40 g/L. The effects of MSA concentrations, anode current density, and temperature on the composition of anode slime and cathode products, anode current efficiency, and energy consumption were investigated in a beaker cell with 500 mL electrolyte. The anode current efficiency and energy consumption were calculated using Eqs. (1) and (2), respectively. The element contents of products, including anode slime and cathode product, were analyzed by ICP and XRF.

$$\eta_a = \frac{m_C}{m_L} \times 100\% \quad (1)$$

$$W = 1000 \times \frac{UIt}{m_L} \quad (2)$$

where $\eta_a$ is anode current efficiency, i.e. the electrorefining efficiency (%); $m_C$ and $m_L$ are the

mass of the cathode product and the anode mass loss, respectively (g); $U$ is the voltage (V); $I$ is the current (A); $t$ is the reaction time (h); $W$ is the DC power consumption (kW·h/t).

2.2.3 Oxidation leaching

The leaching and oxidizing agents are respectively, MSA and hydrogen peroxide, and the scale for the single-factor test is 20 g of the bismuth-enriched anode slime per test. The effect of concentration of MSA, solid/liquid ratio, dosage of the oxidizing agent, leaching time, reaction temperature on leaching efficiency was studied. Equation (3) presents the calculation formula of leaching efficiency. The content of the main element and phase in leachate and leaching residue was analyzed by ICP, XRF, and XRD.

$$\eta_{\mathrm{l}}=\frac{cV}{wm_{\mathrm{B}}}\times 100\% \tag{3}$$

where $\eta_{\mathrm{l}}$ is the leaching efficiency (%); $m_{\mathrm{B}}$ is the mass of the bismuth in anode slime (g); $w$ is the content of the bismuth in anode slime (%); $c$ is the concentration of $Bi^{3+}$ in leaching solution (g/L); $V$ is the volume of the leaching solution (L).

2.2.4 Electrodeposition

With graphite as anode and 316L stainless steel as the cathode, the impacts of concentration of $Bi^{3+}$ and cathode current density on the cathode current efficiency and energy consumption were investigated in a beaker cell with 500 mL simulation electrolyte. The computational formula of cathode current efficiency is shown in Eq. (4). The XRD, XRF, ICP, and SEM were performed to analyze the plates' purity and morphology.

$$\eta_{\mathrm{c}}=\frac{m'_{\mathrm{B}}}{q_{\mathrm{c}}It}\times 100\% \tag{4}$$

where $\eta_{\mathrm{c}}$ is the cathode current efficiency (%); $m'_{\mathrm{B}}$ is the mass of bismuth in the cathode (g); $q_{\mathrm{c}}$ is the electrochemical equivalent for $Bi^{3+}$ to Bi, and the value is 2.599 g/(A·h).

### 2.3 Electrochemical experiment

Electrochemical experiments were performed in a three-electrode cell. A 316L stainless steel electrode (effective area of 7.065 $mm^2$) was used as the working electrode, a high-purity platinum sheet (effective area of 1 $cm^2$) was worked as the auxiliary electrode, and the reference electrode was the saturated calomel (mercurous sulfate) electrode. Before the electrochemical tests, the working electrode was polished with metallographic sandpapers of 1200 and 3500 grit and then rinsed with ethanol solution and distilled water.

## 3 Results and discussion

### 3.1 Process experiment

3.1.1 Electrorefining

3.1.1.1 Single factor test results

Under conditions of a temperature of 30 °C, a cathode current density of 300 A/$m^2$ and a reaction time of 3 h, the anode mass loss, the electrorefining efficiency, and the mass and the element content of anode slime and cathode product were investigated at the MSA concentrations of 1, 2, 3, and 4 mol/L, as demonstrated in Fig. 2 and Table 2.

As the concentration of MSA increases, there is a moderate decline that could be found in the anode mass loss, the mass of anode slime, and the content of lead in anode slime, while the proportion of bismuth in anode slime increases. However, when the MSA concentration exceeds 3 mol/L, the anode mass loss and the lead content in anode slime increase sharply, and the mass of anode slime rises while bismuth content in anode slime drops, indicating that the dissolving capacity of the system to alloy is significantly enhanced. Nevertheless, as the dissolution rate increases, many anode alloys fall into anode slime before completing dissolution, which is not conducive to the lead deposition at the cathode and the separation of lead and bismuth. In addition, with the increase of MSA concentration, the mass of the cathode product generally remains stable at a certain level, and the electrorefining efficiency gradually ascends. However, when the MSA concentration becomes 4 mol/L, the electrorefining efficiency and the product mass decline dramatically with more energy consumption because of anode passivation. Under a condition of high MSA concentration, the purity of lead recovered in the cathode product cannot be guaranteed, while the bismuth recovery increases steeply, even reaching 50%. As a result, the optimum MSA concentration is 3 mol/L.

The effect of current density (300, 400, 500, and 600 A/$m^2$) on the electrorefining process was investigated at 30 °C, an MSA concentration of 3 mol/L, and a reaction time of 3 h. The results are shown in Fig. 3 and Table 2.

**Table 2** Main element contents of anode slime and cathode product in different conditions

| Factor | Value | Content in anode slime/wt.% | | | Content in cathode product/wt.% | | |
|---|---|---|---|---|---|---|---|
| | | Pb | Bi | Sb | Pb | Bi | Sb |
| Concentration of MSA/(mol·L$^{-1}$) | 1 | 19.49 | 58.87 | 10.42 | 75.51 | 23 | 0.42 |
| | 2 | 4.72 | 70.32 | 10.73 | 98.35 | 0.91 | 0.09 |
| | 3 | 3.12 | 73.50 | 10.43 | 96.95 | 2.19 | 0.22 |
| | 4 | 36.23 | 40.62 | 10.87 | 50.12 | 47.05 | 0 |
| Cathode current density/(A·m$^{-2}$) | 300 | 3.12 | 73.50 | 10.43 | 96.95 | 2.19 | 0.22 |
| | 400 | 2.62 | 75.12 | 10.72 | 98.58 | 0.80 | 0 |
| | 500 | 1.81 | 75.31 | 10.43 | 99.43 | 0 | 0 |
| | 600 | 20.31 | 50.42 | 10.41 | 76.51 | 20.52 | 0.12 |
| Temperature/°C | 30 | 3.12 | 73.50 | 10.43 | 98.58 | 0.80 | 0 |
| | 45 | 3.08 | 72.20 | 10.82 | 96.95 | 0.82 | 0 |
| | 60 | 3.02 | 72.13 | 10.72 | 96.56 | 0 | 0 |

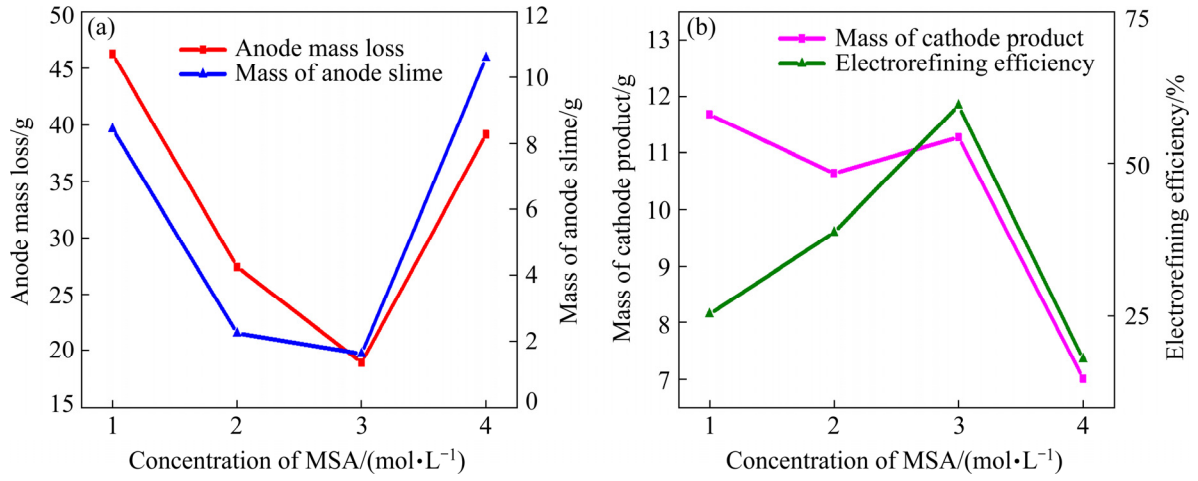


**Fig. 2** Effect of concentration of MSA on electrorefining process: (a) Anode mass loss and mass of anode slime; (b) Mass of cathode product and electrorefining efficiency

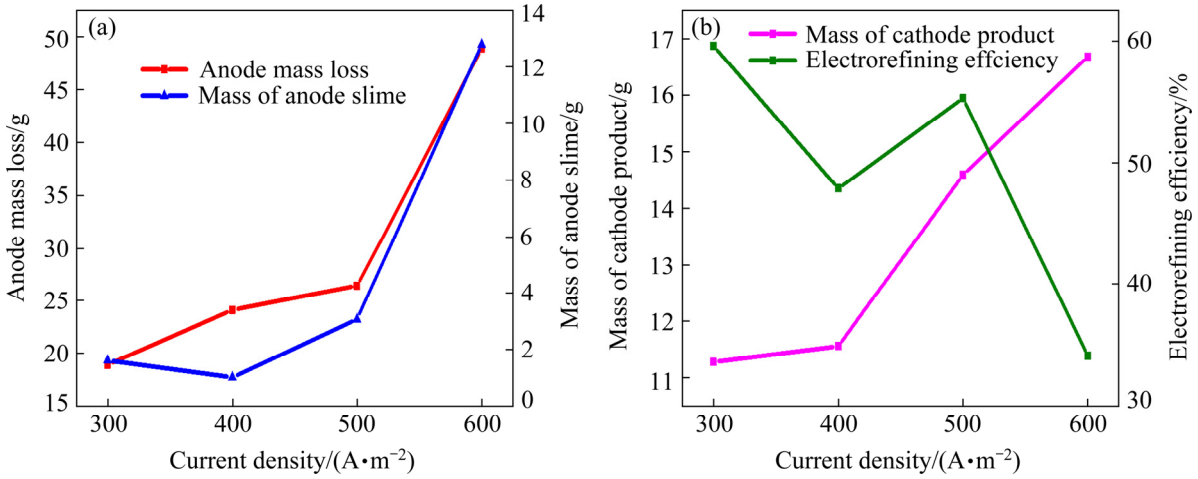


**Fig. 3** Effect of current density on electrorefining process: (a) Anode mass loss and mass of anode slime; (b) Mass of cathode product and electrorefining efficiency

An increase in the current density can improve the capacity of anode dissolving. Meanwhile, the mass of anode slime also exhibits a notable rise. However, when the current density reaches 600 A/m$^2$, the anode slime composition is significantly different from that at other current densities, with prominently higher lead content. As current density increases, the current and voltage also rise to a certain extent, which accelerates the alloy dissolution, making the part of lead components in the alloy fail to start the dissolving reaction timely. Then, the undissolving lead falls into the electrolytic cell along with other unreacted metals. In addition, the overhigh current density may cause the over oxidation of lead to $Pb^{4+}$, and the $Pb^{4+}$ does not dissolve in this system [18,19]. As the current density rises, the mass of the cathode product increases with a ladder-typed increase of electrorefining efficiency. It may be due to the uneven distribution of elements in the preparation process (casting) of the electrolytic anode used. Although we have done several experiments to reduce the experimental errors caused by the uneven distribution of elements in the anode, some errors are still unavoidable. Although lead is the main component in cathode products when the current density is 600 A/m$^2$, high content of bismuth plays an unfavorable role in the subsequent process. This phenomenon results from the promotion of bismuth dissolution caused by the ascension of current density. Since the standard electrode potential of bismuth is higher than that of lead, bismuth deposition is preferred. So, to obtain the cathode product with higher purity in electrorefining, the current density should not be set to be too high. As a result, the cathode current density should not exceed 600 A/m$^2$ during electrorefining, and the optimal value is 500 A/m$^2$.

Three tests at different temperatures were carried out: 30 °C (room temperature), 45 °C (actual production temperature), and 60 °C (high temperature). Furthermore, other conditions were controlled at the current density of 500 A/m$^2$, the MSA concentration of 3 mol/L, and the reaction time of 3 h. The test results are shown in Table 2 and Table 3.

The results demonstrate that temperature variations have no significant effect on the anode mass loss and the mass of cathode products, while they may exhibit some influence on the electrorefining efficiency: both DC power consumption and bismuth content in the cathode decline to some extent. Hence, there is no significant difference in the electrorefining process with temperature changing. It is more appropriate to perform electrorefining at room temperature (30 °C) because of energy saving.

**Table 3** Effect of temperature on electrorefining process

| Temperature/ °C | Anode mass loss/g | Mass of anode slime/g | Mass of cathode product/g | Electrorefining efficiency/ % |
|---|---|---|---|---|
| 30 | 24.11 | 11.56 | 1.02 | 47.90 |
| 45 | 23.50 | 11.85 | 1.35 | 50.43 |
| 60 | 23.33 | 12.70 | 2.08 | 54.40 |

3.1.1.2 Comprehensive condition test results

The optimum condition of electrorefining with a temperature of 30 °C, a current density of 500 A/m$^2$, and an MSA concentration of 3 mol/L was obtained by single-factor test and applied to the comprehensive condition test. The cathode products and anode slime were recovered after performing the electrolysis for 24 h with a cycle period of 8 h. Table 4 reveals the comprehensive condition test results, and Table 5 illustrates the main element contents in anode slime and cathode products.

**Table 4** Comprehensive condition test results of electrorefining

| Anode mass loss/g | Mass of anode slime/g | Mass of cathode product/g | Electro-refining efficiency/% | DC power consumption/ (kW·h·t$^{-1}$) |
|---|---|---|---|---|
| 78.60 | 48.90 | 19.70 | 63.30 | 535.00 |

**Table 5** Main element contents in anode slime and cathode product of comprehensive condition test (wt.%)

| Sample | Pb | Bi | Sb | Ag | Cu |
|---|---|---|---|---|---|
| Anode slime | 2.26 | 75.32 | 10.59 | 6.42 | 3.82 |
| Cathode product | 91.31 | 7.71 | 0.33 | 0 | 0 |

As shown from the above results, the lead powder and bismuth-rich anode slime are obtained through the electrorefining process. The separation of lead, bismuth, and antimony can be effectively achieved. The contents of antimony, lead, and bismuth in lead powder in the cathode are 0.33, 91.31, and 7.71 wt.%, respectively. The contents of bismuth, antimony, and silver in anode slime are

75.32, 10.59, and 6.42 wt.%, respectively, with a lower amount of copper and lead involved.

3.1.2 Oxidation leaching

3.1.2.1 Single factor test results

The oxidation leaching process was studied by adding an oxidant (hydrogen peroxide) to the leaching process. In this process, the oxidation reaction of bismuth in bismuth-rich anode slime occurs, and the bismuth ion enters to solution by the double-replacement reaction between oxidative product and MSA. The test conditions and results are shown in Fig. 4.

As the concentration of MSA increases from 1−4 mol/L (Fig. 4(a)), the concentration of bismuth ions in the solution exhibits a slight rise, and the leaching efficiency of bismuth also changes from

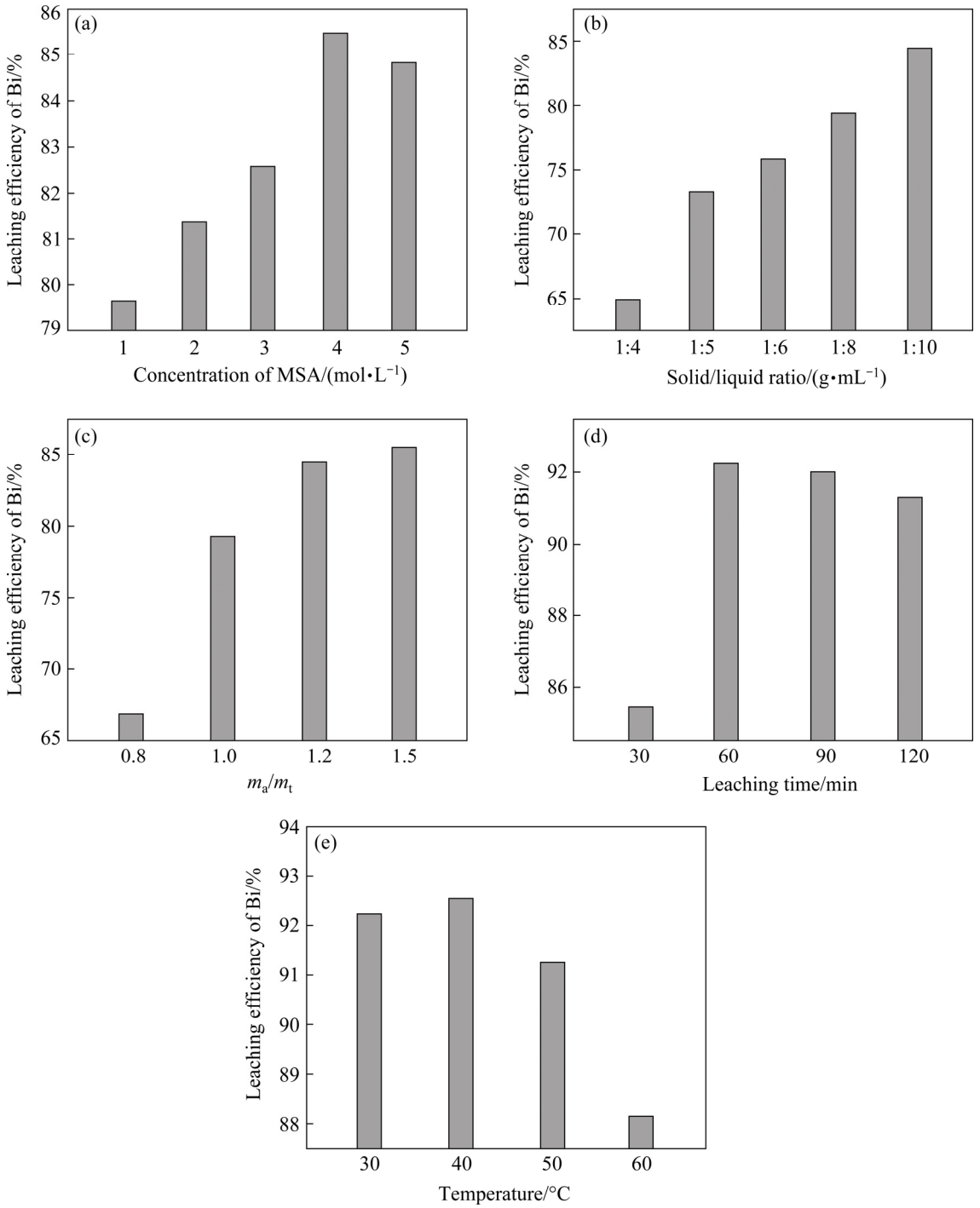


**Fig. 4** Leaching efficiency of Bi under different conditions: (a) 30 °C, solid/liquid ratio S/L=1:10, $m_a/m_t$=1.5 ($m_a$ is actual oxidant dosage; $m_t$ is theoretical oxidant dosage), 30 min; (b) 30 °C, $c$(MSA)=4 mol/L, $m_a/m_t$=1.2, 30 min; (c) 30 °C, $c$(MSA)=4 mol/L, S/L=1:10, 30 min; (d) 30 °C, $c$(MSA)=4 mol/L, S/L=1:10, $m_a/m_t$=1.5; (e) $c$(MSA)=4 mol/L, S/L=1:10, $m_a/m_t$=1.2, 60 min

79.64% to 85.45%. However, when the MSA concentration continues to grow beyond a certain limit (5 mol/L), the leaching efficiency of bismuth shows an opposite trend, with a slight decrease to 84.82%. This phenomenon can be explained by the fact that the leaching reaction is difficult to occur due to the passivation of metals in the high acidity condition. Since the subsequent electrodeposition of bismuth requires certain acidity, the optimal MSA concentration is determined to be 4 mol/L. With an increase in liquid volume (Fig. 4(b)), the leaching efficiency of bismuth gradually rises while the mass of the residue gradually declines. When the solid/liquid ratio reaches 1:10, the leaching efficiency of bismuth climbs to 84.38%. A high liquid/solid ratio results in a large liquor volume, which improves the mixing effect of the anode slime particles and leaching reagent, which is favorable to leaching reaction. Although a high solid/liquid ratio is beneficial to improving the leaching efficiency of bismuth, it also leads to a decrease in the concentration of $Bi^{3+}$ in the solution, which is adverse to the subsequent bismuth's electrodeposition. Therefore, the best solid/liquid ratio is 1:10. Figure 4(c) illustrates that as the dosage of hydrogen peroxide increases, the leaching efficiency of bismuth rises significantly. When the actual amount of hydrogen peroxide is 0.8 times the theoretical amount, the leaching efficiency of bismuth is only 66.78%, which manifests that the bismuth in the raw material cannot be entirely oxidized by hydrogen peroxide. Therefore, an adequate dosage of hydrogen peroxide is the premise of the high leaching efficiency of bismuth. When the oxidant is injected into the anode slime, it may break down before reacting with the bismuth that needs to be oxidized. So, the amount of hydrogen peroxide added during leaching should be higher than the theoretical amount. When the actual amount of hydrogen peroxide is 1.5 times the theoretical value, the leaching efficiency of bismuth reaches the maximum of 85.45%. As a result, the leaching efficiency of bismuth is optimal when the actual amount of hydrogen peroxide is 1.5 times the theoretical value. The leaching efficiency of bismuth reaches the maximum of 92.23% at a leaching time of 60 min (Fig. 4(d)). When the leaching time is more than 60 min, the leaching efficiency of bismuth keeps stable at about 92%. Hence, the optimal leaching time is 60 min. According to Fig. 4(e), with the increase of leaching temperature, the leaching efficiency of bismuth remains stable at first. Furthermore, it decreases with the increase of temperature because the oxidant we choose is hydrogen peroxide, and the oxidant breaks down faster at higher temperatures. When the temperature is higher than 40 °C, hydrogen peroxide's oxidation performance worsens, leading to a low leaching efficiency. As a result, the optimal temperature is 40 °C.

3.1.2.2 Comprehensive condition test results

An expanded comprehensive test was carried out with 50 g of the anode slime as raw material. The test condition was as follows: a temperature of 40 °C, a solid/liquid ratio of 1:10, an MSA concentration of 4 mol/L, a hydrogen peroxide dosage of 1.5 times the theoretical value, and a leaching time of 60 min. When bismuth is leached, it is completely oxidized by adding hydrogen peroxide drop by drop. The test results are shown in Table 6, and the XRD analysis result of the leaching residue is shown in Fig. 5.

It can be seen from Table 6 that the leaching efficiency of bismuth in the comprehensive test is 86.20%, and antimony is basically concentrated in the residue, indicating that the separation of antimony and bismuth is achieved. It is found that the concentration of bismuth in the leaching solution reaches 40.40 g/L, while the concentrations of other metal ions are relatively low, which is

**Table 6** Analysis of element equilibrium during bismuth leaching in comprehensive condition

| Element | Content in anode slime (50 g)/wt.% | Concentration in leaching solution (668 mL)/(g·L$^{-1}$) | Content in leaching residue (18.20 g)/wt.% | Leaching equilibrium | | |
|---|---|---|---|---|---|---|
| | | | | Residue/% | Solution/% | Error/% |
| Bi | 75.32 | 40.40 | 31.20 | 18.14 | 86.20 | +4.34 |
| Sb | 10.59 | 0.02 | 23.10 | 103.60 | − | +3.60 |
| Pb | 2.26 | 1.66 | 0.89 | 12.51 | 85.64 | −2.85 |
| Cu | 3.82 | 0.85 | 1.59 | 38.53 | 66.67 | +5.20 |
| Ag | 6.42 | − | 8.44 | 100 | − | − |

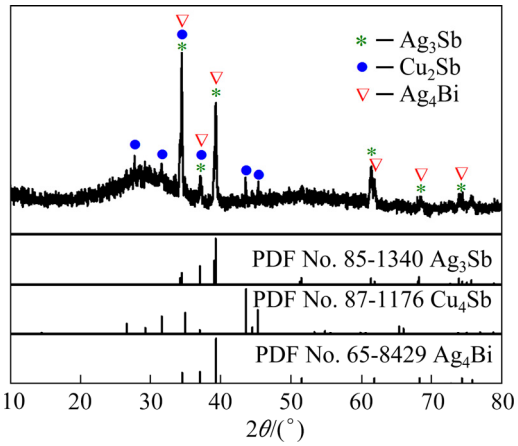


**Fig. 5** XRD pattern of leaching residue under comprehensive condition

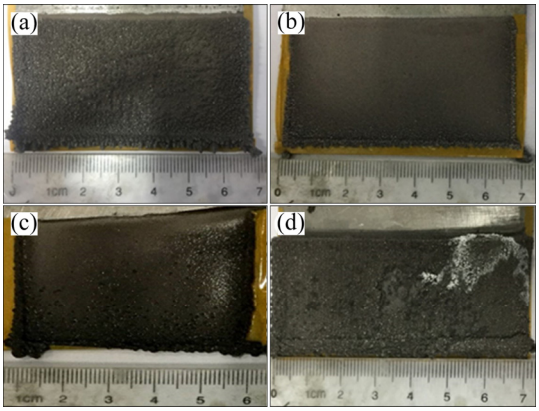


**Fig. 7** Macroscopic morphologies of product at different cathode current densities: (a) 200 A/m$^2$; (b) 300 A/m$^2$; (c) 400 A/m$^2$; (d) 500 A/m$^2$

favorable to the bismuth electrodeposition process. Bismuth accounts for 18.14% of the mass in the residue. Figure 5 illustrates that the bismuth in the residue mainly exists in the form of bismuth silver alloy ($Ag_4Bi$), which is difficult to be oxidized into corresponding metal oxides under the general oxidation conditions, thus resulting in relative difficulties in leaching [20].

3.1.3 Electrodeposition

3.1.3.1 Single factor test results

The bismuth electrodeposition test at different cathode current densities of 200, 300, 400, and 500 A/m$^2$ was performed under a temperature of 30 °C, an MSA concentration of 4 mol/L, a $Bi^{3+}$ concentration of 60 g/L, and a reaction time of 4 h. The results are shown in Figs. 6 and 7.

With the gradual increase of current density, the current efficiency of bismuth electrodeposition moves up first, and then goes down. Under the condition of a cathode current density of 300 A/m$^2$, the current efficiency of bismuth electrodeposition reaches the maximum of 98.74%. When the cathode current density continues to grow, the cathode current efficiency gradually declines due to hydrogen evolution promoted by high current densities. Both metal deposition and hydrogen evolution reactions occur on the cathode, so the current efficiency of metal deposition will drop. Optical photographs of the corresponding electrodeposited products at different current densities demonstrate that the bismuth plates produced by electrodeposition are compact and smooth when the current density is 300 A/m$^2$. However, the bismuth plate becomes porous and fluffy when the current density is more than 300 A/m$^2$, illustrating an inferior plate forming effect. Therefore, the optimal cathode current density is 300 A/m$^2$.

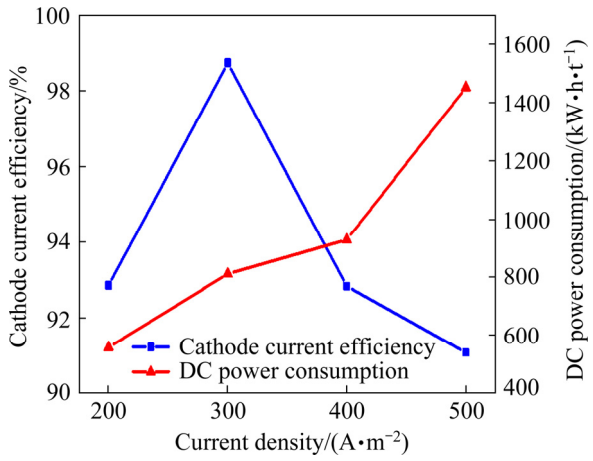


**Fig. 6** Effect of current density on cathode current efficiency and DC power consumption

Figures 8 and 9 reveal the bismuth electrodeposition test results under a temperature of 30 °C, an MSA concentration of 4 mol/L, a reaction time of 4 h, and $Bi^{3+}$ concentrations of 40, 60, 80, and 100 g/L.

Figure 8 shows that the current efficiency at cathode gradually rises as the concentration of bismuth ion increases. When the concentration of bismuth ion exceeds 60 g/L, the cathode current efficiency fluctuates slowly. When $Bi^{3+}$ concentration surpasses 80 g/L, the cathode current efficiency is close to 100%. After calculation, the cathode current efficiency can even reach 101% when the $Bi^{3+}$ concentration is 100 g/L, which is unreasonable. This is because a small amount of

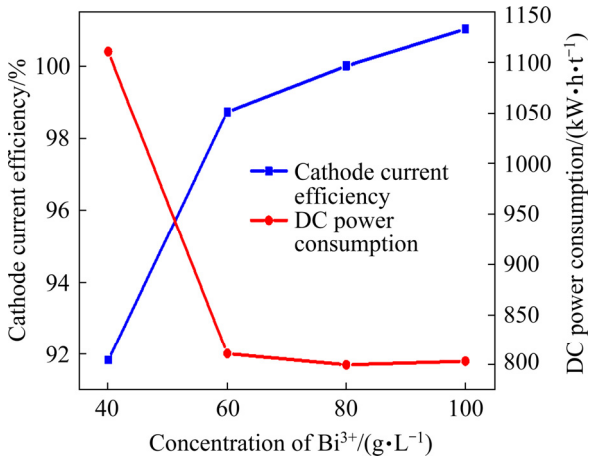


**Fig. 8** Effect of concentration of $Bi^{3+}$ on cathode current efficiency and DC power consumption

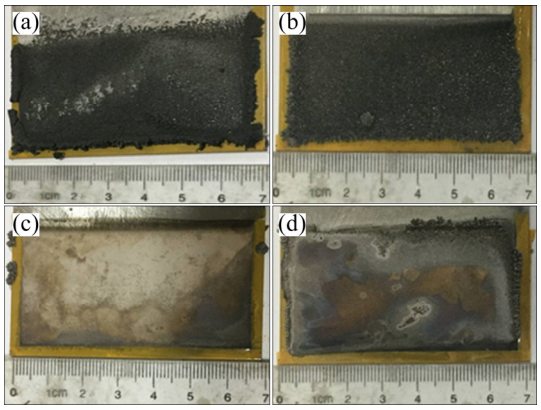


**Fig. 9** Macroscopic morphologies of cathode at different concentrations of $Bi^{3+}$: (a) 40 g/L; (b) 60 g/L; (c) 80 g/L; (d) 100 g/L

bismuth may be oxidized on the bismuth plate's surface during the processes of acquiring, stamping, and drying. When the concentration of $Bi^{3+}$ in the system is low, hydrogen evolution takes place preferentially on the cathode, resulting in increased energy consumption and poor morphology (Figs. 8 and 9). When the concentration of $Bi^{3+}$ increases to a certain value sufficient $Bi^{3+}$ capable of acquiring electrons near the cathode will inhibit hydrogen evolution reaction. As a result, higher bismuth ion concentration of 60−100 g/L will result in better electrodeposition.

3.1.3.2 Comprehensive condition test results

Electrolyte for comprehensive tests was the leaching solution obtained from the leaching process of oxidative anode slime. The electrodeposition was carried out for 6 h at 30 °C and a cathode current density of 300 A/m$^2$. The process parameters of the comprehensive condition test for bismuth electrodeposition and the cathode bismuth composition are reported in Tables 7 and 8, respectively. Figure 10 presents the macroscopic morphology and SEM images of the cathode bismuth plate, while Fig. 11 reveals the XRD patterns of cathode bismuth. It should be noted that the concentration of $Bi^{3+}$ in the leaching solution reached 93.36 g/L in the comprehensive condition test, which was obtained by cyclic leaching (the condition of cyclic leaching is the optimal condition, which obtained by single-factor test. The first leaching solution was returned to leach raw

**Table 7** Process parameters of bismuth electrodeposition comprehensive conditions test

| Average current/A | Average voltage/V | Cathode current efficiency/% | DC power consumption/(kW·h·t$^{-1}$) |
|---|---|---|---|
| 0.39 | 1.50 | 92.45 | 624.50 |

**Table 8** Main element contents of cathode bismuth (wt.%)

| Bi | Pb | Cu | Sb | Ag |
|---|---|---|---|---|
| 99.80 | 0.057 | 0.073 | 0.010 | 0.003 |

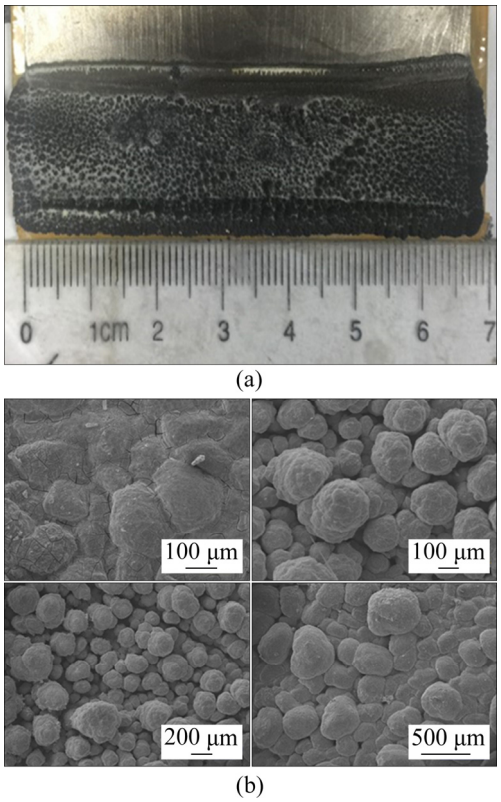


**Fig. 10** Macroscopic morphology (a) and SEM images (b) of cathode bismuth in comprehensive condition

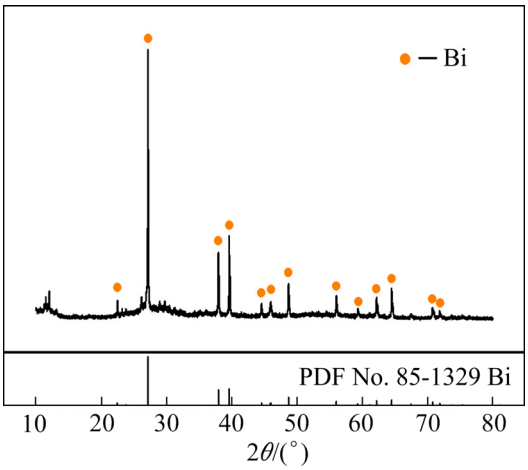


**Fig. 11** XRD patterns of cathode bismuth under comprehensive condition

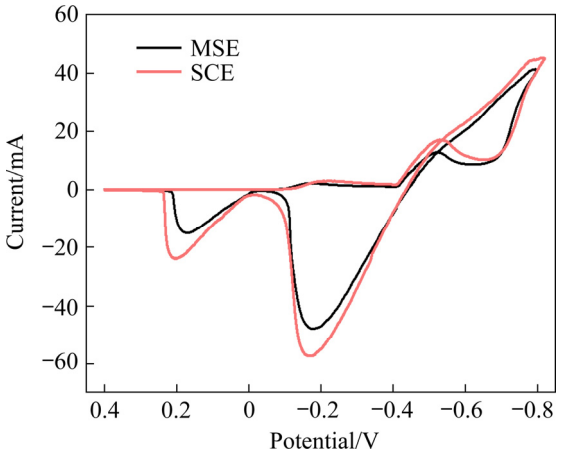


**Fig. 12** Cyclic voltammetry curves using different reference electrodes after processing

bismuth-rich anode slime, and it will repeat three times to achieve the purpose of enrichment of $Bi^{3+}$).

The comprehensive condition test shows that the bismuth plate obtained from the leaching solution possesses a dense morphology, and the bismuth plate's purity can reach 99.80%. Nevertheless, the SEM images show that the bismuth plate's morphology is spherical, especially on the edge of the plate. The spherical structure makes it difficult for bismuth to grow at the plate, and the main reason for the spherical structure is that the additive fails to act fully in the electrodeposition.

### 3.2 Electrochemical experiment results

The electrochemical tests were performed to investigate the reaction mechanism and the ion chemical behavior at the cathode in the electrorefining process to get the cathode product with high purity.

3.2.1 Cyclic voltammetry

Firstly, the effect of different reference electrodes on the results of the electrochemical test was investigated. SCE and MSE were used as reference electrodes for the test at a temperature of 35 °C, a $Bi^{3+}$ concentration of 15 g/L, a $Pb^{2+}$ concentration of 75 g/L, an MSA concentration of 4 mol/L, and a scanning rate of 100 mV/s. After the test, the standard electrode potential obtained at 35 °C with SCE as the reference electrode was taken as a reference, and the experimental results with MSE as the reference electrode were processed (0.480 V). The results are shown in Fig. 12.

It can be seen from Fig. 12 that, without considering the difference in the standard potential of the reference electrode, the curves obtained by using MSE and SCE as reference electrodes have a similar trend. When MSE is used as the reference electrode, the peak intensity (area) of bismuth and lead is lower than that of SCE. The MSE is filled with the $K_2SO_4$ saturated solution. At the beginning of the experiment, a small amount of $SO_4^{2-}$ entered into the solution through the reference electrode and reacted with $Pb^{2+}$ and $Bi^{3+}$ to precipitate, which reduced the concentration of metal ions and thus affected the intensity of precipitation peak (area) of Pb and Bi. Secondly, a small amount of $Cl^-$ will not precipitate with $Pb^{2+}$ because of the higher solubility of $PbCl_2$ (compared with $PbSO_4$). Meanwhile, $Cl^-$ will gradually move towards the anode after entering the solution, so the influence on the cathode reaction is not significant. Therefore, we chose SCE as the reference electrode for the following electrochemical tests.

The cyclic voltammetry curves are shown in Fig. 13, with different scanning rates (5, 10, 20, 50, and 100 mV/s) at 35 °C, a $Bi^{3+}$concentration of 15 g/L, a $Pb^{2+}$concentration of 75 g/L, and an MSA concentration of 4 mol/L.

For the cyclic voltammetry curve obtained with the scanning rate of 5 mV/s, a reduction peak is observed at around −0.05 V (vs SCE) when the scanning potential moves from positive to negative. According to the standard electrode potentials of metals, Bi deposition should occur at first. As the scanning potential continues to move toward a negative direction, a prominent reduction peak

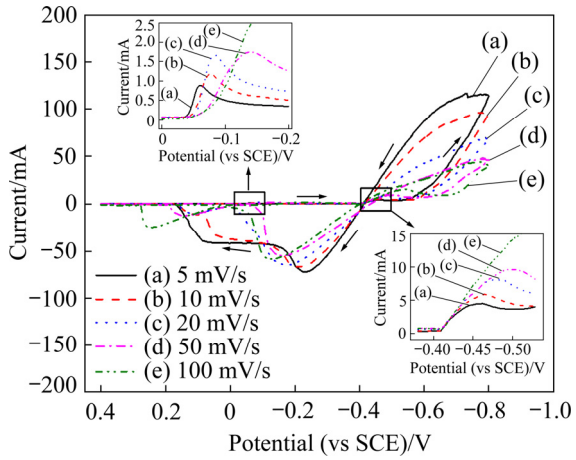


**Fig. 13** Cyclic voltammetry curves at different scanning rates

is found at about −0.42 V (vs SCE), where Pb deposition should occur. The scanning potential continues towards the negative direction, and when the potential is −0.57 V (vs SCE), the current suddenly increases, illustrating the occurrence of hydrogen evolution. When the scanning potential starts to return, the current is 0 at the potential of −0.40 V (vs SCE), suggesting the beginning of the electrorefining process. As the scanning potential goes back to the positive, two peaks representing metal dissolution appear, corresponding to lead and bismuth. The peak currents of bismuth and lead electrodeposition gradually climb with increasing the scanning rate, and the peak potential also changes. The calculation formulas of the potential peak for reversible and irreversible reactions are shown in Eqs. (5) and (6), respectively. The former potential does not change with scanning rate, while the latter is related to the scanning rate, suggesting that electrodeposition and reduction of bismuth and lead are irreversible [21].

$$\varphi_p=\varphi_{1/2}-1.109\frac{RT}{nF} \tag{5}$$

$$\varphi_p=\varphi^{\Theta}-\frac{RT}{\alpha F}\left[0.780+\ln\frac{D_0^{1/2}}{k_0}+\ln\left(\frac{\alpha Fv}{RT}\right)^{1/2}\right] \tag{6}$$

where $\varphi_p$ is the peak potential (V); $\varphi_{1/2}$ is the half peak potential (V); $R$ is the molar gas constant (J/(mol·K)); $T$ is the temperature (K); $n$ is the number of electrons gained; $F$ is the Faraday's constant (C/mol); $\varphi^{\Theta}$ is the standard electrode potential (V); $\alpha$ is the transfer coefficient; $D_0$ is the diffusion coefficient ($m^2/s$); $k_0$ is the reaction rate constant; $v$ is the scanning rate (mV/s).

For an irreversible reaction, the relationship between the scanning rate and the peak current ($I_p$) complies with Eq. (7):

$$I_p=2.99\times10^5 nAC_0\alpha^{1/2}D_0^{1/2}v^{1/2} \tag{7}$$

where $I_p$ is the limiting current density ($mA/m^2$); $A$ is the dimensionless frequency factor; $C_0$ is the initial concentration of metallic ion concentration.

The fitting curve between the scanning rate's square root and the peak current is plotted in Fig. 14.

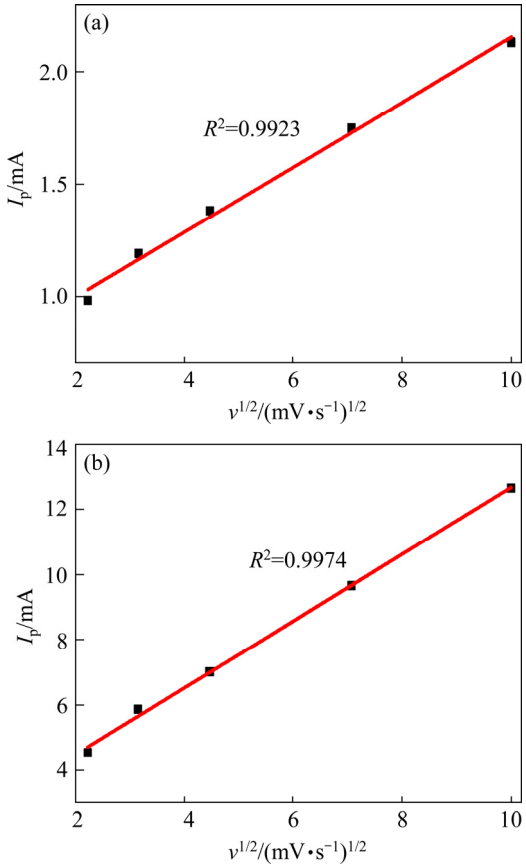


**Fig. 14** Diagrams showing relationship between reduction peak currents and square root of scanning rates: (a) Bi; (b) Pb

In Fig. 14, there are suitable fittings between peak currents and scanning rates, with fitting coefficients of 0.9923 and 0.9974 for Bi and Pb, respectively, indicating that the metals (Bi and Pb) deposition reactions in the electrorefining process are controlled by diffusion [22,23].

3.2.2 Linear polarization

3.2.2.1 Effect of temperature on electrorefining

The cathode polarization curves at a $Bi^{3+}$ concentration of 15 g/L, a $Pb^{2+}$ concentration

of 75 g/L, an MSA concentration of 4 mol/L, a scanning rate of 50 mV/s, and temperatures of 20, 35, 45, and 55 °C are shown in Fig. 15.

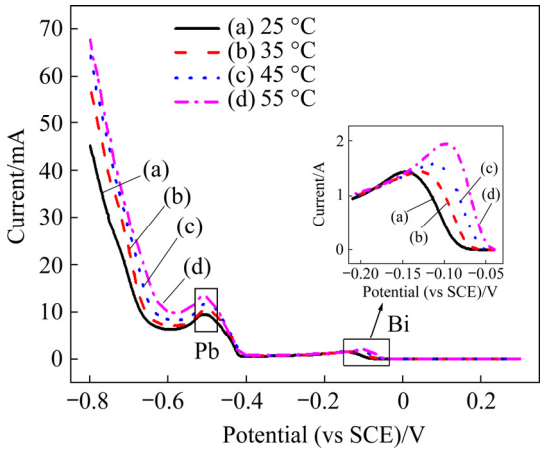


**Fig. 15** Cathode polarization curves at different temperatures

Two peaks appear as the potential decreases, and these two peaks are the deposition peaks of bismuth and lead, respectively. When the temperatures are 25, 35, 45, and 55 °C, the initial reduction potentials of bismuth are −0.080, −0.060, −0.040, and −0.030 V (vs SCE), respectively. In contrast, the initial reduction potentials of lead are stable, at about −0.425 V. This phenomenon clarifies that increasing temperature has little effect on the initial reduction potential of lead, but it is beneficial to bismuth deposition. Because the ion moves slowly at a low reaction temperature, and a more significant potential is needed as a driving force to enable $Bi^{3+}$ to reach the cathode and participate in the reaction. However, due to the high concentration of $Pb^{2+}$ in the solution, there are many $Pb^{2+}$ ions near the cathode taking in the reaction, which do not affect the reduction potential obviously. In addition, with increasing the temperature, the reduction currents of bismuth and lead increase to a certain extent, indicating that the reaction will be accelerated by rising temperature due to the speed-up of ion movement. Therefore, a low temperature is not conducive to the electrorefining reaction and the bismuth deposition. As a result, the electrorefining process should be conducted at a lower temperature to improve the lead's purity in the cathode product.

3.2.2.2 Effect of $H^+$ concentration on electrorefining

The cathodic polarization curves at a $Bi^{3+}$concentration of 15 g/L, a $Pb^{2+}$ concentration of 75 g/L, a temperature of 35 °C, a scanning rate of 50 mV/s, and MSA concentrations of 1, 2, 3, and 4 mol/L are shown in Fig. 16.

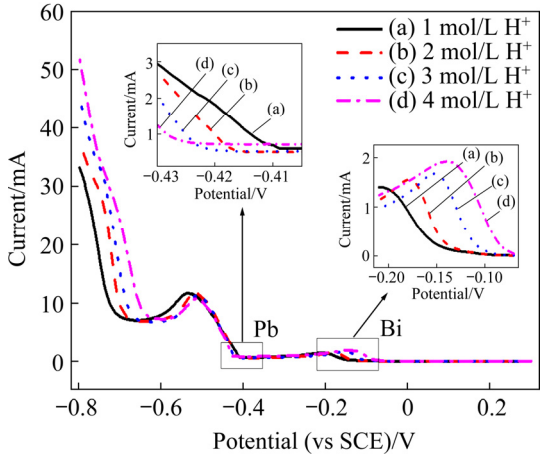


**Fig. 16** Cathode polarization curves at different acidities

With the increase of the concentration of $H^+$ (1, 2, 3, and 4 mol/L), the initial reduction potentials of bismuth increase, and the values are −0.140, −0.120, −0.100, and −0.080 V (vs SCE), respectively. This indicates that a high concentration of $H^+$ favors bismuth deposition. However, the initial reduction potentials of lead decrease from −0.410 to −0.425 V (vs SCE) when the concentration of $H^+$ climbs from 1 to 4 mol/L, which illustrates that lead can be deposited more quickly in the low acidity condition. Based on the comparison of the change of the initial reduction potentials of bismuth and lead, different change trends of the initial reduction potentials of lead and bismuth can explain the electrode property of the cathode. With the deposition of bismuth, the electrode property of the cathode will change to the steel−bismuth alloy, and the high the bismuth content is, the lower the conductivity is, so it is necessary to decrease the content of bismuth in the cathode electrode [24]. In addition, the potential of hydrogen evolution reaction on the cathode will decrease with the increase of $H^+$ concentration. When the concentrations of $H^+$ are 1, 2, 3, and 4 mol/L, the potentials of hydrogen evolution reaction are −0.705, −0.672, −0.635, and −0.600 V (vs SCE), respectively. This indicates that $H^+$ has a noticeable effect on electrorefining. The above analysis reveals that the low concentration of $H^+$ inhibits bismuth deposition and hydrogen evolution by increasing the reduction potential and promotes lead deposition by decreasing the reduction

potential. As a result, the electrorefining should be carried out under a low concentration of MSA, which can improve the purity of lead in the cathode and inhibit hydrogen evolution reaction to improve the current efficiency.

## 4 Conclusions

(1) A new hydrometallurgical process based on the methanesulfonic acid system can extract bismuth effectively from the by-products (lead alloy bearing high bismuth and antimony) of lead smelting.

(2) The optimal conditions of the whole processes are as follows: for the electrorefining process, the bismuth-rich anode slime and the raw lead powder were obtained at an MSA concentration of 3 mol/L, a cathode current density of 500 A/m$^2$, and a temperature of 30 °C; for the oxidation leaching process, the leachate and antimony−silver residue were obtained at an MSA concentration of 4 mol/L, a solid/liquid ratio of 1:10, a hydrogen peroxide dosage of 1.5 times of the theoretical amount, a leaching time of 60 min, and a temperature of 40 °C; for the bismuth electrodeposition process, the cathode bismuth with the current efficiency of 92.45% and the purity of 99.8% was obtained at a cathode current of 300 A/m$^2$, and a concentration of $Bi^{3+}$ larger than 60 g/L.

(3) During the electrorefining process, three reactions occur at the cathode, namely lead deposition, bismuth deposition, and hydrogen evolution, and the reactions of metals deposition are both irreversible and diffusion-controlled. In addition, decreasing the temperature and acidity can improve the purity of the cathode product in the electrorefining process.

## Acknowledgments

The authors are grateful for the financial supports from the National Key Research and Development Program of China (No. 2018YFC1900403).

## References

[1] PENG Z W, MACKEY P J. New developments in pyrometallurgy [J]. JOM, 2013, 65: 1550−1551.

[2] ZHANG Zhe-qiu, YUAN Lu-cheng, HUANG Lin-qing, XU Zhi-feng. Trend and recovery of arsenic, antimony and bismuth in copper smelting [J]. Nonferrous Metals Science and Engineering, 2019, 10(1): 13−19. (in Chinese).

[3] LUDVIGSSON B M, LARSSON S R. Anode slimes treatment: The boliden experience [J]. JOM, 2003, 55: 41−44.

[4] WU Wen-hua, WANG Zhi-jian, LIU Ji-bo. Hydro-metallurgical pretreatment process for the recovery of valuable metals from the lead anode slime [J]. Advanced Materials Research, 2013, 813: 153−156.

[5] NAKANO A, ROCHMAN N T, SUEYOSHI H. Removal of lead from copper alloy scraps by compound-separation method [J]. Journal of the Japan Institute of Metals, 2005, 46(12): 2719−2724.

[6] CAO Hua-zhen, CHEN Jin-zhong, YUAN Hai-jun, ZHANG Guo-qu. Preparation of pure $SbCl_3$ from lead anode slime bearing high antimony and low silver [J]. Transactions of Nonferrous Metals Society of China, 2010, 20(12): 2397−2403.

[7] LIU Wei-feng, YANG Tian-zu, ZHANG Du-chao, CHEN Lin, LIU Yun-feng. A new pyrometallurgical process for producing antimony white from by-product of lead smelting [J]. JOM, 2014, 66: 1694−1700.

[8] XIONG Heng, YANG Bin, LIU Da-chun, XU Bao-qiang, CHEN Xiu-min, DENG Yong. Copper-based multi-component alloys by vacuum distillation to separate copper enriched lead, silver and other valuable metals [C]//Proceedings of the 4th International Symposium on High-temperature Metallurgical Processing. San Antonio, TX: TMS, 2013: 255−264.

[9] HE Yun-long, XU Rui-dong, HE Shi-wei, ZHU Yun, SHEN Qing-feng, CHEN Han-sen, LI Kuo. Research development of lead anode slime treatment technology [J]. Nonferrous Metals Science and Engineering, 2017, 8(5): 40−51. (in Chinese).

[10] CHEN Ya, LIAO Ting, LI Gai-bian, CHEN Bai-zhen, SHI Xi-chang. Recovery of bismuth and arsenic from copper smelter flue dusts after copper and zinc extraction [J]. Minerals Engineering, 2012, 39(12): 23−28.

[11] LUCHEVA B, ILIEV P, KOLEV D. Hydro-pyrometallurgical treatment of copper converter flue dust [J]. Journal of Chemical Technology and Metallurgy, 2017, 52(2): 320−325.

[12] LITTLE H F V, CAHEN E. The separation of bismuth from lead, and the analysis of bismuth−lead alloys [J]. Analyst, 1910, 35(14): 301−306.

[13] FAN Jin-long, WANG Gang, LI Qing, YANG Hao-wei, XU Shuo, ZHANG Jie, CHEN Jin-wei, WANG Rui-lin. Extraction of tellurium and high purity bismuth from processing residue of zinc anode slime by sulfation roasting — leaching — electrodeposition process [J]. Hydrometallurgy, 2020, 194: 105348.

[14] TANAKA T. Adhesion of anode slime on anode surface in electrolytic refining of lead [J]. Metallurgical Transactions B, 1977, 8(3): 651−660.

[15] IVANOV I, STEFANOV Y, NONCHEVA Z, PETROVA M, DOBREV T, MIRKOVA L, VERMEERSCH R, DEMAEREL J P. Insoluble anodes used in hydrometallurgy: Part II. Anodic behaviour of lead and lead-alloy anodes [J]. Hydrometallurgy, 2000, 57(2): 125−139.

[16] PENG Si-yao, YANG Jian-guang, YANG Jian-ying, LEI Jie. The recovery of bismuth from bismuthinite concentrate through membrane electrolysis [C]//Proceedings of the Rare Metal Technology 2017. San Diego, CA: TMS, 2017: 285−301.
[17] GERNON M D, WU M, BUSZTA T, JANNEY P. Environmental benefits of methanesulfonic acid: Comparative properties and advantages [J]. Green Chemistry, 1999, 1(3): 127−140.
[18] VELICHENKO A B, DEVILLIERS D. Electrodeposition of fluorine-doped lead dioxide [J]. Cheminform, 2007, 128(4): 269−276.
[19] XIAO Fa-xin, ZHENG Ya-jie, JIAN Hong-sheng, GONG Zhu-qing, XU Wei. Influence of As, Sb and Bi on electrodepositing and anode oxidation mechanism of copper [J]. Journal of Central South University (Science and Technology), 2009, 40(3): 575−580. (in Chinese)
[20] MATSUSHIMA K, OHTSUKI T. On the growth of silver−bismuth alloy deposits on a rock salt [J]. Journal of Vacuum Science and Technology, 1970, 7(1): 107−110.
[21] BARD A J, FAULKNER L R. Electrochemical methods: Fundamentals and applications [M]. 2nd ed. New York: John Wiley and Sons, 2001.
[22] NAN Tian-xiang, YANG Jian-guang, CHEN Bin. Electrochemical mechanism of tin membrane electrodeposition under ultrasonic waves [J]. Ultrasonics Sonochemistry, 2018, 42: 731−737.
[23] LEI Jie, YANG Jian-guang. Electrochemical mechanism of tin membrane electro-deposition in chloride solutions [J]. Journal of Chemical Technology and Biotechnology, 2016, 92(4): 861−867.
[24] KIKUCHI K. Material performance in lead and lead−bismuth alloy [J]. Comprehensive Nuclear Materials, 2012, 5: 207−219.

# 基于甲基磺酸体系从铅冶炼副产物中湿法提铋

南天翔[1]，杨建广[1]，唐朝波[1]，汪文超[1]，龙 伟[1]，杨济源[2]

1. 中南大学 冶金与环境学院，长沙 410083；
2. 西北工业大学 伦敦玛丽女王大学工程学院，西安 710129

**摘 要：**为有效提取铅冶炼副产物中的铋，提出一种基于甲基磺酸体系的湿法提铋新工艺。提铋工艺包括电精炼、氧化浸出和电沉积。通过单因素试验确定提取铋的最佳工艺条件。在最优工艺条件下，得到纯度为 99.8%的铋板。采用循环伏安法和线性扫描伏安法研究电解精炼的阴极反应机理。结果表明，铅和铋的沉积及氢析出反应均为不可逆反应，且反应的控制步骤为扩散控制；另外，电解精炼过程中，较低的反应温度和酸度可以提高阴极铅粉的纯度。

**关键词：**铋；湿法冶金工艺；甲基磺酸体系；电化学机理

**(Edited by Wei-ping CHEN)**